Second-harmonic generation from regeneratively amplified femtosecond laser pulses in BBO and LBO crystals

Jing-yuan Zhang

Department of Physics, Georgia Southern University, Ladrum Box 8031, Statesboro, Georgia 30460

Jung Y. Huang

Institute of Electro-optical Engineering, National Chiao Tung University, Taiwan

H. Wang, K. S. Wong, and G. K. Wong

Department of Physics, Hong Kong University of Science and Technology, Kowloon, Hong Kong

Received May 12, 1997; revised manuscript received September 3, 1997

The spectral and temporal characteristics and optical-conversion efficiency of ~150-fs laser pulses at 400 nm generated by second-harmonic generation (SHG) of a regeneratively amplified mode-locked Ti:sapphire laser were investigated both theoretically and experimentally. The theoretical investigation was done by taking into account cubic nonlinearity, pulse walk-off, group-velocity dispersion, Kerr nonlinearity, quadratic broadening, frequency chirping of the fundamental pulse, and higher-order nonlinear mixing such as backconversion and optical parametric processing. The experimental studies of the effects of crystal length and pumping intensity on the pulse duration, the spectrum, and the optical-conversion efficiency of the SHG were carried out in BBO and LBO crystals of various thicknesses and compared with the theory. It was found that in a nontransform-limited pulse, the most significant contribution to the temporal and spectral distortion of the ~150-fs SHG pulses is mainly due to the chirping of the fundamental beam and self-phase modulation at high pumping intensity and long crystal length. The optimum crystal length and pumping intensity for obtaining a high optical-conversion efficiency and a pure spectrum in SHG are also calculated and experimentally investigated. It was found that a transform-limited fundamental pulse is essential to obtain a high conversion efficiency and to preserve the temporal profile of the second-harmonic pulse. It is also found that for a nontransform-limited ~150-fs pulse, a 0.5–0.6-mm BBO crystal and a modest pumping intensity of ~40 GW/cm^2 are the most suitable for SHG. [S0740-3224(98)02001-3]

OCIS codes: 190.0190, 190.4160, 320.2250.

1. INTRODUCTION

Recent advances in ultrashort-pulse generation and amplification have resulted in near-IR pulses directly from a mode-locked Ti:sapphire laser and regenerative amplifier with output energy ranging from microjoules to a few tens of millijoules and pulse duration of the order of 10–100 fs, tunable from 720 nm to 950 nm.[1–4] It is of considerable interest to extend the tuning range of the Ti:sapphire laser to the visible and UV regions with equally short pulse durations without significant spectral distortion. For example, one can convert the tunable output of a Ti:sapphire laser into the blue or the UV by second-harmonic generation (SHG), or more generally, by sum-frequency generation (SFG). The ultrashort pulses in the blue or in the UV can then be used as the pumping source for other nonlinear optical-frequency extension devices, such as the optical parametric oscillator, the optical parametric generator (OPG), the optical parametric amplifier, and the difference-frequency generator. The outputs from SHG and the above-mentioned devices are continuously tunable from the UV to the mid IR. SHG (or SFG) is an essential step to convert ultrashort laser pulses from the visible and the near-IR regions to shorter wavelength range. The most important issue in SHG (or SFG) of the ultrashort pulses is the preservation of the pulse duration, bandwidth, and simultaneous achievement of a reasonable optical efficiency. Frequency-conversion processes often lead to pulse broadening and frequency chirping. These effects are even worse inside a laser cavity where a light pulse travels through a cavity several times. Fortunately, these effects can be removed with an insertion of a wavelength-dependent optical delay line (e.g., a prism or grating pair) in the laser cavity. Even so, in a mode-locked laser or a regenerative amplifier, asymmetric, double-peaked, and other distorted spectra have still been observed and predicted.[5–6] The above-mentioned technique, however, does not work properly for an amplified ultrashort laser with low (~10 Hz) to medium repetition rate (~1 kHz). The frequency conversion in these cases is normally implemented with a single-pass traveling wave scheme where the peak power of laser pulses is usually high enough to generate nonnegligible frequency chirping, pulse broadening, and other nonlinear optical effects. These side effects cannot be easily removed without introducing extra energy loss.

0740-3224/98/010200-10$10.00

To achieve high efficiency conversion in SHG (or SFG) without significant degradation in the spectral and temporal characteristics of the converted pulses, a detailed analysis is required.

Some theoretical work has been done recently to investigate the effects of group-velocity dispersion,[7–10] intrapulse group-velocity dispersion, and various orders of nonlinear phases[11–12] to the pulse duration of the frequency-doubled pulses. Some experimental work has involved the study of the optical efficiency of SHG of ultrashort pulses[13,14] and the optical-conversion limits.[8,10] Experimental and theoretical studies of various effects, which affect the optical-conversion efficiency, pulse width, especially the distortion of spectral distribution, are of great importance and have not been done in detail so far, to our knowledge. In this paper, we present systematic theoretical and experimental studies of the effects that cause significant pulse broadening (or shortening), distortion of the spectrum, and the limit of optical-conversion efficiency in the SHG of ~150-fs pulses.

This paper is organized as follows: In Section 2 we give a numerical model by taking into account some essential effects such as cubic nonlinearity, pulse walk-off group-velocity dispersion, quadratic broadening, and frequency chirping in the SHG processes. In Section 3, we first present the data of theoretical calculations on the temporal characteristics of the second harmonic (SH) pulse from transform-limited and non-transform-limited fundamental pulses by taking into account group-velocity dispersion, pulse walk-off, self-phase modulation, frequency chirping of input pulse, and quadratic broadening, and we then make comparisons with the experimental SH pulse shapes measured by cross correction between the SH pulse and the fundamental pulse. The studies are then focused on the spectral distortion of the SH output by considering higher-order nonlinear mixing, quadratic broadening, and self-phase modulation with transform-limited and non-transform-limited pulses. The comparisons are then made between the theoretical results and the experimental SH spectra measured in several crystals at various pumping intensities. The optical effects that affect the optical-conversion efficiency are then investigated by considering all the above-mentioned effects including Kerr nonlinearity. The experimental measurements were made in BBO and LBO crystals with various crystal lengths to find suitable crystal lengths and pumping intensities to achieve high conversion without significant temporal and spectral degradation. Finally, the conclusion, with some discussions on optimizing crystal length and pumping intensity, are given in Section 4.

2. NUMERICAL MODEL

To understand the essential effects of cubic nonlinearity, pulse walk-off, and group-velocity dispersion on frequency conversion of ultrashort laser pulses, we start with the scalar wave equations governing the propagation of the drive wave and its second harmonic through a nonlinear crystal with second- and third-order nonlinearities:

$$\frac{\partial^2 E}{\partial z^2} - \mu_0\epsilon_0 \frac{\partial^2 E}{\partial t^2} - \mu_0 \frac{\partial^2 P_{\mathrm{L}}}{\partial t^2} = \mu_0 \frac{\partial^2 P_{\mathrm{NL}}}{\partial t^2}, \qquad (1)$$

where $E = E_1 + E_2$ with E_1 and E_2 being the electric fields of the fundamental and the second-harmonic pulses, respectively. The linear and the nonlinear polarizations are denoted by $P_{\mathrm{L}} = \epsilon_0\chi^{(1)}E^{(1)}$ and $P_{\mathrm{NL}} = \epsilon_0\chi^{(2)}E^{(2)} + \epsilon_0\chi^{(3)}E^3$, respectively. Under the plane-wave approximation, E_1 and E_2 then can be written as

$$E_1(z, t) = \frac{1}{2}\bar{E}_1 \exp[i(\omega_1 t - k_1 z)] + \text{c.c.},$$

$$E_2(z, t) = \frac{1}{2}\bar{E}_2 \exp[i(2\omega_1 t - k_2 z)] + \text{c.c.}. \qquad (2)$$

By substituting Eq. (2) into Eq. (1) and then invoking the slowly varying amplitude approximation, we can obtain coupled-wave equations that have the following expressions:

$$\frac{\partial \bar{E}_1}{\partial z} + \frac{1}{v_{1g}}\frac{\partial \bar{E}_1}{\partial t} + ig_\omega \frac{\partial^2 \bar{E}_1}{\partial t^2} = \frac{i\omega\chi^{(2)}}{2n_\omega c}\bar{E}_1^*\bar{E}_2 + \frac{i\omega\chi^{(3)}}{2n_\omega c}\left[\frac{3}{4}|\bar{E}_1|^2 + \frac{3}{2}|\bar{E}_2|^2\right]\bar{E}_1,$$

$$\frac{\partial \bar{E}_2}{\partial z} + \frac{1}{v_{2g}}\frac{\partial \bar{E}_2}{\partial t} + ig_{2\omega} \frac{\partial^2 \bar{E}_2}{\partial t^2} = \frac{i\omega\chi^{(2)}}{2n_{2\omega} c}\bar{E}_1^{\,2} + \frac{i\omega\chi^{(3)}}{n_{2\omega} c}\left[\frac{3}{2}|\bar{E}_1|^2 + \frac{3}{4}|\bar{E}_2|^2\right]\bar{E}_2, \qquad (3)$$

where $v_{ig} = c/n_{ig}$ with $n_{ig} = n_i + \omega_i(\partial n/\partial\omega)|_{\omega_i}$ is the group velocity and $g_n = 0.5(\partial^2 k/\partial\omega^2)|_{\omega_n}$ is the dispersion-spreading coefficient. The pulse distortion caused by the self-phase modulation ($\chi^{(3)}|E_i|^2E_i$) and the cross-phase modulation ($\chi^{(3)}|E_i|^2E_j$) have been properly taken into account by the second and third terms of Eq. (3). Since the photon energies of the fundamental and the second-harmonic pulses are much smaller than the electronic bandgap of BBO and LBO, the third-order nonlinear response should be much faster than the pulse duration and therefore can be neglected. This also allows us to express the nonlinear of refraction n_2 of material as $n_2(\omega) = \chi^{(3)}/(2n_\omega)$ and $n_2(2\omega) = \chi^{(3)}/(2n_{2\omega})$ in terms of a nondispersive third-order nonlinearity.

It is convenient to transform Eq. (3) into a pulse-moving frame and then convert it into a dimensional form by properly choosing normalization parameters that include nonlinear interaction length $z_i = 2n_\omega c/(\omega\chi^{(2)}E_{10})$, input electric amplitude E_{10}, and pulse duration τ_0. The resulting equations have the following forms of

$$\frac{\partial \tilde{E}_1}{\partial l} + \frac{z_I}{l_w}\frac{\partial \tilde{E}_1}{\partial \bar{\tau}} + \frac{iz_I}{4l_{d1}}\frac{\partial^2 \tilde{E}_1}{\partial \bar{\tau}^2} = i\tilde{E}_1^*\tilde{E}_2 + 2\pi i(n_2E_{10}^2)(z_I/\lambda)\left[\frac{3}{4}\left|\tilde{E}_1\right|^2 + \frac{3}{2}\left|\tilde{E}_2\right|^2\right]\tilde{E}_1,$$

$$\frac{\partial \tilde{E}_2}{\partial l} + \frac{iz_I}{4l_{d2}}\frac{\partial^2 \tilde{E}_2}{\partial \bar{\tau}^2} = i\frac{n_\omega}{n_{2\omega}}\tilde{E}_1{}^2 + 4\pi i(n_2 E_{10}{}^2)(z_I/\lambda) \times \left[\frac{3}{4}|\tilde{E}_2|^2 + \frac{3}{2}|\tilde{E}_1|^2\right]\tilde{E}_2, \quad (3')$$

where $\tilde{E}_i = \bar{E}_i/\bar{E}_{10}$, $l = z/z_I$, and $\bar{\tau} = \tau/\tau_0$, $l_w = c\tau_0/(n_{1g} - n_{2g})$ is the pulse walk-off distance, and $l_d = \tau_0^2/(4g)$ denotes the pulse-spreading distance. Equation (3) needs to be solved numerically. We use a symmetric split-step beam-propagation method to obtain general solutions for these equations. In this approach, nonlinear coupled Eqs. (3) are divided into a dispersion part,

$$\frac{\partial \tilde{E}_1}{\partial l} + \frac{z_I}{l_w}\frac{\partial \tilde{E}_1}{\partial \bar{\tau}} + \frac{iz_I}{4l_{d1}}\frac{\partial^2 \tilde{E}_1}{\partial \bar{\tau}^2} = 0,$$

$$\frac{\partial \tilde{E}_2}{\partial l} + \frac{iz_I}{4l_{d2}}\frac{\partial^2 \tilde{E}_2}{\partial \bar{\tau}^2} = 0, \quad (4)$$

and a nonlinear part,

$$\frac{\partial \tilde{E}_1}{\partial l} = i\tilde{E}_1^*\tilde{E}_2 + 2\pi i(n_2 E_{10}{}^2)(z_I/\lambda) \times \left[\frac{3}{4}|\tilde{E}_1|^2 + \frac{3}{2}\left|\tilde{E}_2\right|^2\right]\tilde{E}_1,$$

$$\frac{\partial \tilde{E}_2}{\partial l} = i\frac{n_\omega}{n_{2\omega}}\tilde{E}_1{}^2 + 4\pi i(n_2 E_{10}{}^2)(z_I/\lambda) \times \left[\frac{3}{4}|\tilde{E}_2|^2 + \frac{3}{2}|\tilde{E}_1|^2\right]\tilde{E}_2, \quad (5)$$

to govern pulse evolution inside each distance increment $(l, l + \mathrm{d}l)$. Inside each distance increment, we need three steps to obtain the output pulse envelopes at $l + \mathrm{d}l$ from their values at l. During step 1 in $(l, l + \mathrm{d}l/2)$, a fourth-order Runge–Kutta algorithm is applied to solve Eqs. (4) with initial values of $\tilde{E}_1(l)$ and $\tilde{E}_2(l)$. For step 2 at $l + \mathrm{d}l/2$, Eq. (5) is then solved with a fast Fourier transform technique through $\hat{E}(l, f) = \int \tilde{E}(l, \bar{\tau})\exp(2\pi i f\bar{\tau})\mathrm{d}\bar{\tau}$ to yield

$$\hat{E}_1(l + \mathrm{d}l, f) = \hat{E}_1(l, f)\exp\left[2\pi i f\left(\frac{z_I}{l_w} + \frac{\pi f z_I}{2l_{d1}}\right)\mathrm{d}l\right],$$

$$\hat{E}_2(l + \mathrm{d}l, f) = \hat{E}_2(l, f)\exp\left[2\pi i f\left(\frac{\pi f z_I}{2l_{d2}}\right)\mathrm{d}l\right]. \quad (6)$$

The solutions account for the pulse walk-off and pulse-spreading effects from the crystal slice of $(l, l + \mathrm{d}l)$. The resulting spectra are then inverse transformed back to the time domain. In step 3, step one is repeated with the new envelopes obtained in step 2 as the initial values, which evolve into pulse envelopes from $l + \mathrm{d}l/2$ to $l + \mathrm{d}l$. These three steps are sequentially repeated until the whole crystal is propagated through. Such an implementation yields a numerical model of frequency conversion with ultrashort pulses that is mathematically simple and numerically efficient.

An amplified ultrashort pulse from a nonideal pulse compressor often exhibits a non-transform-limited envelope. To investigate the frequency-conversion processes with a non-transform-limited pulse, we model the input-pulse envelope with an expression of

$$\bar{E}_1(0, \bar{\tau}) = E_{10}\exp\left[-\frac{\bar{\tau}^2}{(1 + i4f_2)}\right]. \quad (7)$$

This envelope form implies a pulse with a duration–bandwidth product of one of the following:

$$\tau_0\Delta f_B = \frac{2\ln 2}{\pi}\sqrt{1 + (4f_2)^2},$$

$$\tau_0\frac{\Delta\lambda}{\lambda_0} = \frac{2\lambda_0\ln 2}{c\pi}\sqrt{1 + (4f_2)^2}. \quad (8)$$

Note that, for a non-transform-limited 150-fs laser pulse that has a central wavelength of 800 nm and a full width at half-maximum of the spectrum, $\Delta\lambda = 8$ nm can then be modeled with a quadratic spectral broadening of $f_2 = 0.2$.

3. THEORETICAL CALCULATIONS AND EXPERIMENTAL RESULTS

A. Experimental Arrangement

The experimental arrangement is shown in Fig. 1. Briefly, an Ar-ion laser is used to pump a mode-locked Ti:sapphire laser (Coherent Mira 900) whose output is amplified by a YLF-laser-pumped Ti:sapphire regenerative amplifier (made by Quantronix) operating at 1 kHz. The output of the regenerative amplifier is ~400 mW, corresponding to 400 μJ per pulse, at a wavelength of approximately 800 nm with a pulse duration of 150 fs and a FWHM bandwidth of ~8 nm. Roughly 20% of the output of the regenerative amplifier is used for cross correlation to measure the pulse duration of the SH pulses, and the residual output is telescoped down by a 1:10× telescope to reach a maximum power density of more than 150 GW/cm^2. The beam cross section is elliptical with dimensions 0.705 mm (horizontal) × 0.445 mm (vertical).

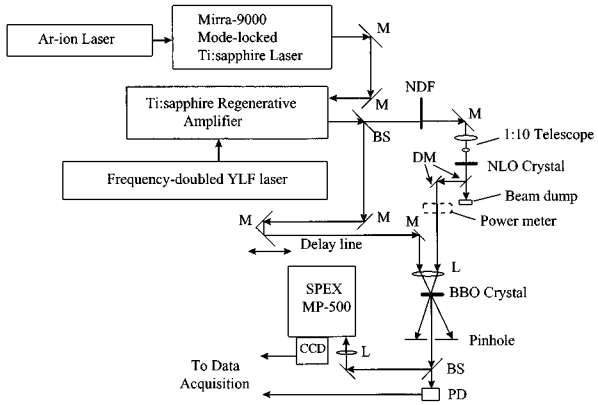

Fig. 1. Experimental arrangement for the study of temporal and spectral characteristics of the SHG of ultrashort pulses.

The pumping intensity is adjusted by inserting a continuously adjustable neutral-density filter. BBO and LBO crystals with various thicknesses are used as the nonlinear media for SHG. The output of SHG, after removing the residual pump beam with two dichroic mirrors, is then measured by a powermeter to find the conversion efficiency or spectrally analyzed by a CCD spectrometer (SPEX HR-500 and Spectrum One) to monitor the change of the spectrum. Pulse duration of the SHG is measured by cross correlation between the pulses from the fundamental beam at 800 nm and the pulses from the output of SHG in a 1-mm BBO crystal.

B. Comparison of the Theoretical Calculation with the Experimental Results

1. Temporal Characteristics of Second-Harmonic Pulse

The preservation of the temporal and spectral characteristics of a femtosecond laser pulse is one of the important issues in frequency conversion, including for SHG, SFG, DFG, and OPG. For time-resolved spectroscopic applications, laser pulses with well-defined temporal and spectral characteristics are needed. With this point of view in mind, we numerically investigate the temporal and spectral properties of SH pulse from type I BBO crystals pumped by 150-fs pulses at 800 nm.

Figure 2 presents the theoretical cross-correlation profiles of the output SH field with the input fundamental pulse by use of varying thicknesses of BBO and the efficiency of SHG as a function of crystal length. The input fundamental pulse is transform limited ($f_2 = 0$). In each figure panel, the solid, dashed, and short-dashed curves denote the results with the pump intensity being chosen at very high (120 GW/cm^2), medium (40 GW/cm^2), and low (7 GW/cm^2) levels, respectively. For comparison, the autocorrelation profile of the input fundamental pulse is also shown with a dotted curve in Fig. 2(b), where a 0.5-mm BBO is assumed in the calculation, and in other theoretical pulse shapes with longer crystals [1.0-mm BBO in Fig. 2(c) and 2.0-mm BBO in Fig. 2(d)]. The pulse-spreading distance at the second harmonic l_d is as long as 4.3 cm; thus with the crystal lengths used the pulse broadening from group-velocity dispersion can be neglected. Figure 2(a) shows the optical-conversion efficiency of SHG as a function of crystal length at various pumping intensities. Since the nonlinear interaction length $z_l = 0.02$ cm at a high pumping level (for example, at $I_p = 120$ GW/cm^2) is shorter than the pulse walk-off distance ($l_w = 0.07$ cm), the fundamental pulse is depleted significantly within the first 0.07-cm crystal slice near the entrance surface of BBO. No parametric backconversion is possible for a transform-limited pulse. Therefore at a high excitation level the BBO crystals generate SH pulses with nearly the same pulse profile as that of the pumping laser pulse at the fundamental frequency. When the nonlinear interaction length z_I is longer than the pulse walk-off distance (for example, $z_I = 0.09$ cm at a low pumping level of 7 GW/cm^2), the group-velocity difference between the second-harmonic and the fundamental wave broadens the second-harmonic pulse profile if the crystal length is longer than the pulse walk-off distance [see Figs. 2(c) and 2(d)]. In this case, as can be seen from Fig. 2(a), the conversion efficiency increases monotonically with crystal length, but this is done at the price of degradation of the temporal characteristics of the SH pulse. The calculation indicates that, for a transform-limited pulse, a shorter crystal length with a high pumping level is desirable if higher-order nonlinear optical processes (e.g., self- and cross-phase modulation and optical parametric processes) have not been set in. With the measured value of $n_2 = 0.45 \times 10^{-15}$ cm^2/GW for BBO, we estimate the nonlinear phase shift in a 1-mm-long BBO crystal at a pumping level of 120 GW/cm^2 to be less that 45°. Thus the effects of self-phase modulation and cross-phase modulation are negligible under these experimental conditions.

The situation changes when frequency chirping appears in an amplified ultrashort pulse, which may originate from the use of an imperfect pulse compressor. To

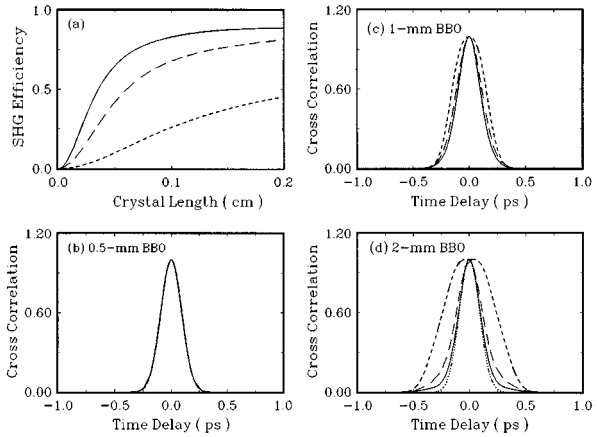

Fig. 2. Calculated results of optical-conversion efficiency as a function of (a) crystal length and cross-correlation profiles of the SHG pulse with a transform-limited femtosecond laser with a pulse duration of 150 fs at three pumping intensities: 7 GW/cm^2 (short-dashed curve), 40 GW/cm^2 (dashed curve), and 120 GW/cm^2 (solid curve) in (b) 0.5-mm BBO, (c) 1.0-mm BBO, and (d) 2.0-mm BBO.

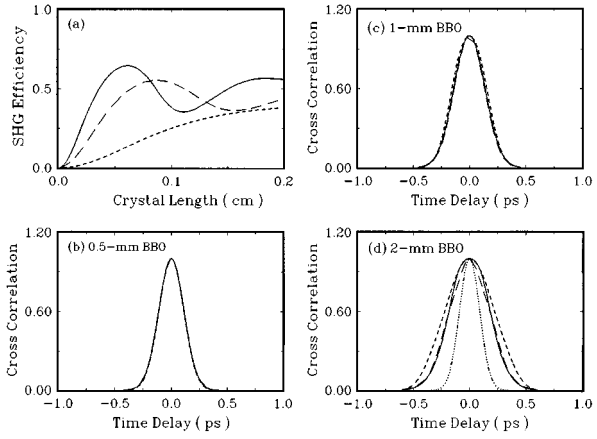

Fig. 3. Calculated results of optical-conversion efficiency as a function of (a) crystal length and cross-correlation profiles of SHG pulse with a non-transform-limited femtosecond laser with a pulse duration of 150 fs at three pumping intensities: 7 GW/cm^2 (short-dashed curve), 40 GW/cm^2 (dashed curve), and 120 GW/cm^2 (solid curve) in (b) 0.5-mm BBO, (c) 1.0-mm BBO, and (d) 2.0-mm BBO.

reveal the effect of frequency chirping on the pulse duration, we perform a calculation by using a non-transform-limited pulse with quadratic spectral broadening $f_2 = 0.2$. The results are shown in Fig. 3. Figure 3(a) shows the optical-conversion efficiency of SHG as a function of crystal length. Instead of a monotonic increase with crystal length as shown in the transform-limited case [see Fig. 2(a)], the optical-conversion efficiency oscillates as the crystal length increases, especially when the pumping intensity is high. The details will be discussed later. The calculated pulse profiles of the SHG under various conditions are shown in Figs. 3(b)–3(d), where three pumping levels are chosen, with the short-dashed curve representing 7 GW/cm^2, the dashed curve representing 50 GW/cm^2, and the solid curve representing 120 GW/cm^2. The dotted curve indicates the autocorrelation profile of the input fundamental pulse. Similar to the situation in Fig. 2, longer crystals and higher pump intensities lead to shorter SH pulses. However, the preservation of a SH temporal profile at high pump intensities is not as effective as that with a transform-limited pulse. Also, the use of high pumping intensity would create spectral distortion and broaden the spectrum of the SH pulse, as will be discussed next.

The experimental cross-correlation profiles of the SHG pulse at various pumping intensities in BBO crystals with thicknesses of 0.5 mm, 1.0 mm, and 2.0 mm are shown in Figs. 4(a)–4(c), while the corresponding profiles for LBO crystals with thicknesses of 1 mm and 3 mm are shown in Figs. 4(d) and 4(e). The cross-correlation profiles show that there is indeed no significant change in the pulse duration in the shortest 0.5-mm BBO crystal when the pumping intensity is increased from 8.6 GW/cm^2 to more than 130 GW/cm^2. However, for the longest 2-mm BBO, the pulse duration of the generated SH pulse at a higher pumping intensity is shorter than that at a lower pumping intensity. On the other hand, the duration of the SH pulse at a low pumping intensity (8.6 GW/cm^2) from a long crystal (for example, a 2-mm BBO) is longer than that from a thin (0.5 mm) BBO at the same pumping intensity. Also, severe degradation in the temporal characteristics of the SH pulse can be readily seen from the pulse profiles generated from a longer crystal at various pumping intensity, indicating that the self- and cross-phase modulation have been set in. All these experimental results agree well with the theoretical calculations shown in Fig. 3.

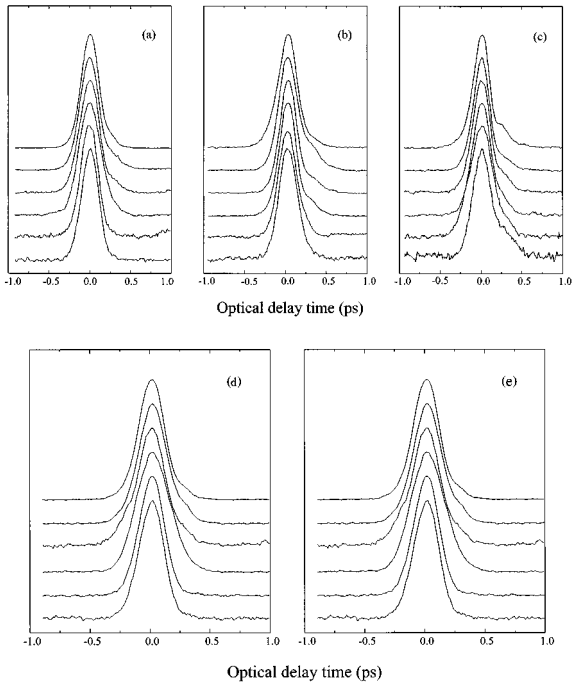

Fig. 4. Experimental cross-correlation profiles of SHG pulses at various pumping intensities obtained from a BBO crystal with various thicknesses: (a) 0.5 mm, (b) 1.0 mm, and (c) 2.0 mm. The pumping intensities (from bottom up) are 8.6, 14.9, 45.6, 81.6, 110, and 132 GW/cm^2. Also shown are experimental cross-correlation profiles of SHG pulses obtained at various pumping intensities from LBO crystal with different thickness: (d) 1.0 mm and (e) 3.0 mm. The pumping intensities (from bottom up) are 8.6, 14.9, 45.6, 81.6, 110, and 132 GW/cm^2.

It is clear that to preserve the temporal profile of the SH pulse it is easier to use a transform-limited pulse than a non-transform-limited pulse. In the latter case, a short crystal and a moderate intensity is preferred.

2. Spectral Characteristics of the Second-Harmonic Pulse

The calculated spectral profiles of the SH pulses with a transform-limited fundamental beam at three pumping intensities in three crystals lengths are shown in Fig. 5, with the short-dashed curve denoting 7 GW/cm^2, the dashed curve denoting 50 GW/cm^2, and the solid curve denoting 120 GW/cm^2. Since the spectral bandwidth for the SHG process is inversely proportional to crystal length, the spectral width of the SH pulse becomes narrower in a longer crystal at low pumping level, for example, for FWHM bandwidths of 3.23 nm, 2.55 nm, and 1.57 nm for the 0.5-, 1.0-, and 2.0-mm BBO's, respectively [see the short-dashed curves in Fig. 5(a)–5(c)]. However, at high pump intensity, the spectral wings of the SH pulse from a 2-mm BBO increase with the pumping intensity and finally achieve a spectral bandwidth similar to that from the 0.5-mm crystal; thus the output SH pulse from the 2-mm crystal retains a spectral bandwidth similar to that from the 0.5-mm crystal. Note that the spectral peak of the output SH pulse at high and low pump intensity are located at the same wavelength.

With a non-transform-limited fundamental input pulse properly described by $f_2 = 0.2$, the calculated spectral profile of the SH output from a crystal (longer than 1 mm) excited at a high pump intensity was found to be significantly different from that excited at a low pump intensity, as shown in Fig. 6. In addition to the much broader and complicated spectral profile, the spectral peak shifts to a longer wavelength region, indicating that complicated parametric backconversion and sum-frequency-mixing processes occur among the spectral components during the pulses propagation through the nonlinear optical crystal. These complicated optical processes, which occur at high intensity and long crystal length, cause an energy redistribution of all the frequency components involved and shift the spectral peak of the SH pulse to the red. It is noted that some smaller peaks on both sides of the central wavelength of SH pulse can be seen at high

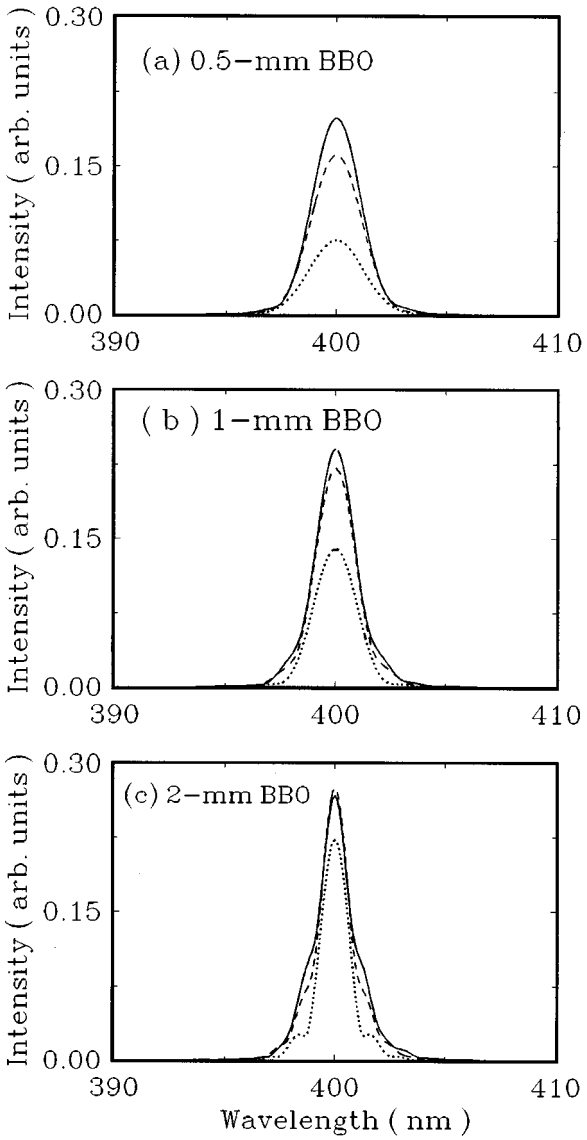

Fig. 5. Calculated spectral profiles of SHG obtained by a transform-limited femtosecond laser at 800 nm at various pumping intensities: (a) 7 GW/cm^2 (short-dashed curve), (b) 40 GW/cm^2 (dashed curve), and (c) 120 GW/cm^2 (solid curve).

pumping intensities, especially in a long crystal. The appearance of side peaks can also be understood as spectral redistribution that is due to the higher-order nonlinear interaction. Therefore it is expected that when a 0.5-mm crystal (shorter than the pulse walk-off distance) is used, a clean spectral profile of the SH pulse can be obtained even at high pump intensities. By comparing Figs. 5 and 6, it is clearly seen that the frequency chirping of the fundamental pulse plays an important role in generating these extra frequency components, especially at high pumping intensities, at which the higher-order nonlinear optical interactions become significant, and in a long crystal, in which phase modulation takes place.

The experimental measurements of the SHG spectra obtained from BBO crystals with various crystal thicknesses as a function of the pumping intensity are shown in Figs. 7(a)–7(c). It is seen from these figures that the spectral behavior of SH pulses from BBO crystals follows the predictions of the theoretical calculations fairly well: First, the spectrum generated from a longer crystal is narrower than that generated from a shorter crystal, especially at a low pumping intensity, where no further spectral complication is introduced by self-phase modulation. Second, the spectra are much broader and complicated at high pumping intensities than at low pumping intensities, especially when a long crystal is used. The spectral distortion and broadening indicate that significant self-phase modulation occurs in the frequency-conversion processes of ultrashort pulses. To preserve the spectral characteristics of the fundamental beam in the SH beam, neither a long crystal nor a high pumping intensity is recommended. Finally, as predicted in the theoretical calculation, the red shift of the SHG peak at high pumping intensities is indeed observable experimentally from the SH spectra measured. The red shift becomes significant as the pumping intensity increases.

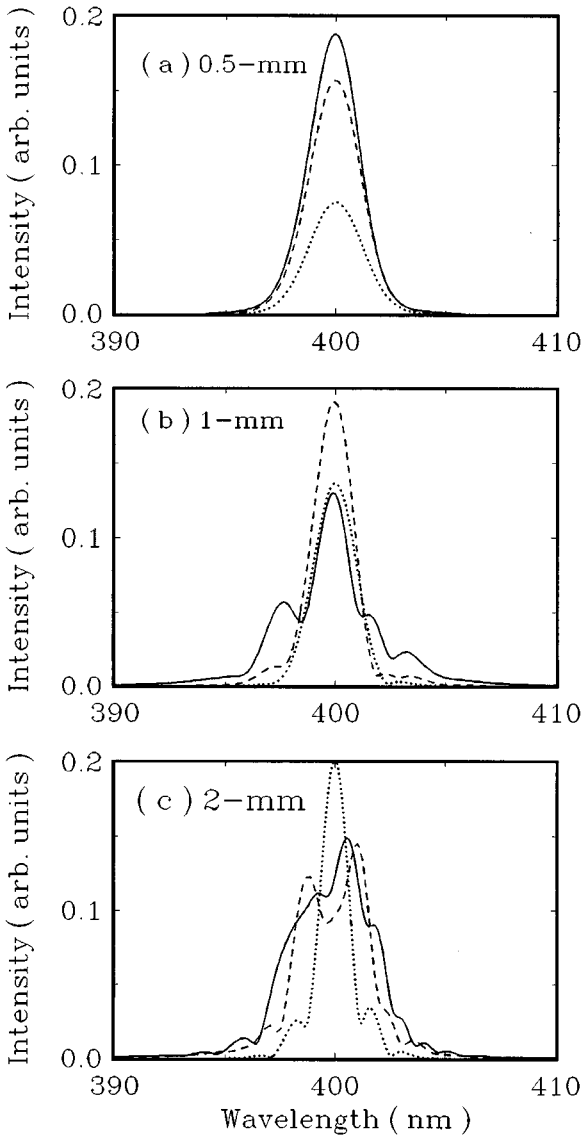

Fig. 6. Calculated spectral profiles of SHG obtained by a nontransform-limited femtosecond laser at 800 nm at various pumping intensities: (a) 7 GW/cm^2 (short-dashed curve), (b) 40 GW/cm^2 (dashed curve), and (c) 120 GW/cm^2 (solid curve).

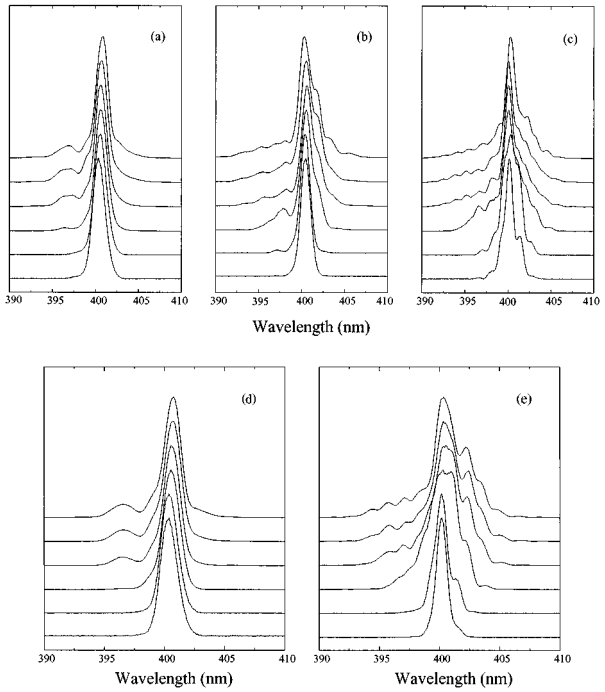

Fig. 7. Experimental spectra of SHG obtained at various pumping intensities from BBO crystals with various thicknesses: (a) 0.5 mm, (b) 1.0 mm, and (c) 2.0 mm. The pumping intensities (from bottom up) are 8.6, 14.9, 45.6, 81.6, 110, and 132 GW/cm^2, respectively. Also shown are experimentally measured spectra of SHG obtained at various pumping intensities from LBO crystals with different thicknesses: (d) 1.0 mm and (e) 3.0 mm. The pumping intensities (from bottom up) are 8.6, 14.9, 45.6, 81.6, 110, and 132 GW/cm^2.

This indicates that the red shift is a higher-order nonlinear effect that is due probably to the strong frequency mixing appearing at high pumping intensities, and the spectral redistribution caused by the self-phase modulation during the pulses propagates through the nonlinear optical crystal, as mentioned earlier. Similar SHG spectra are also seen from the LBO crystals at high pumping intensities. The details are shown in Figs. 7(d) and 7(e). It is clear from Fig. 7 that significant asymmetric spectral distortions occur with pumping intensities higher than 45 GW/cm^2 in all three crystals used. The side peaks in the SH spectra, as predicted in the calculation shown in Fig. 6, are readily observable at high pumping intensities in all three BBO and two LBO crystals.

To avoid spectral distortion in the SH pulse, it is desirable to use transform-limited pulses. With non-transform-limited pulses, a short BBO (0.5–0.6 mm) and a pumping intensity of less than 45 GW/cm^2 work well.

3. Some Optical Effects that Affect the Optical-Conversion Efficiency

Optical-conversion efficiency is one of the most important issues in SHG. High optical-conversion efficiency in SHG of femtosecond pulses can be achieved by selecting appropriate crystals and pumping intensity. In a previous work, we have achieved ~40% optical-conversion efficiency in a 0.5-mm BBO by frequency doubling the output of a 10-Hz Ti:sapphire regenerative amplifier with a fundamental output of ~2.5 mJ per pulse.[15] A 35% conversion efficiency was also reached by Rodriquez *et al.*[14] in a 1.5-mm KDP crystal by frequency doubling a low-repetition regenerative Ti:sapphire laser, which produces an output energy of 100 mJ. A recent work by Krylov *et al.*[10] demonstrated an optical efficiency of ~50% in KDP crystals with thicknesses of 5 mm and 10 mm by means of a ~150-fs Ti:sapphire regenerative amplifier system with energy of 0.6 mJ operating at 1 kHz. In the following, we discuss some optical effects that affect the optical-conversion efficiency of SHG of ~150-fs pulses.

Dependence of SH conversion efficiency on pumping intensity and crystal length: Effects of frequency chirping and quadratic broadening on SHG of transform- and non-transform-limited pulses. Considering the case of SHG in a type I BBO crystal with an amplified Ti:sapphire laser, the calculated SH conversion efficiency as a function of crystal length and pump intensity is presented in Fig. 8, in which the fundamental laser pulse at 800 nm is non transform limited with a quadratic spectral broadening of $f_2 = 0.2$. The crystal can achieve collinear phase matching at $\theta = 29.03°$ and $\varphi = 30°$ with an effective second-order nonlinearity of $d_{\text{eff}} = 1.38$ pm/V. As can be seen from Fig. 8, at low pump intensity (<10 GW/cm^2), the SH-conversion efficiency increases monotonically as the crystal length increases. At a higher pumping intensity, an optimum crystal length, at which the conversion efficiency is maximized, can be seen. The conversion efficiency shows an oscillatory behavior as the crystal length increases. This is expected because a reversal in energy conversion from the SHG back to the fundamental in a non-transform-limited pulse would occur if the SHG pulse becomes sufficiently strong. Owing to the spatial and temporal intensity variations of the fundamental pulse and the phase modulation across the envelope of the electric field of the fundamental beam, parametric backconversion from the SH pulse to the fundamental wave, nonlinear parametric processes and frequency mixings occur. Energy conversion is expected to be different for different parts of the beam, so that the contrast of maxima and minima in the oscillation of the output or conversion efficiency as shown in Fig. 8 is highly smeared. At high pumping intensity, for example, at a pump intensity higher than 100 GW/cm^2, a SH-conversion peak at a crystal length of 0.06 cm is found. This optimum crystal length matches the pulse walk-off length $l_w = 0.068$ cm for 150-fs pulse and is clearly seen in Fig. 8 at high pump intensity.

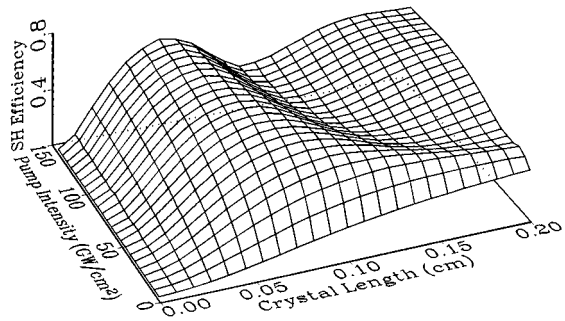

Fig. 8. Theoretical calculation of optical-conversion efficiency of SHG as a function of the crystal length and the laser pumping intensity with a non-transform-limited laser pulse with $f_2 = 0.2$.

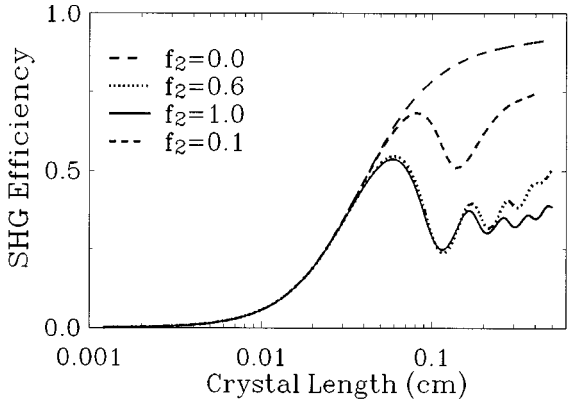

Fig. 9. Theoretical prediction of optical-conversion efficiency of SHG in BBO as a function of the crystal length at various degrees of frequency chirping.

The influence of frequency chirping in a non-transform-limited fundamental pulse on SH conversion can be more clearly observed from the theoretical calculation shown in Fig. 9, where the SH-conversion efficiency as a function of crystal length with varying degrees of quadratic spectral broadening f_2 is shown. In the calculations, the pump intensity and the optical Kerr nonlinearity (which will be discussed next) are fixed to be 120 GW/cm^2 and $n_2 = 0.45 \times 10^{-15}$ cm^2/W. With a transform-limited pump pulse ($f_2 = 0$), the SH-conversion efficiency monotonously increases with crystal length. However, by including frequency chirping in the pump pulse ($f_2 \neq 0$), parametric backconversion is generated. The shortest crystal length for a SH-conversion peak is mainly determined by the pulse walk-off distance.

Owing to the limited nonlinear crystals available, we were unable to carry out a detailed study of the effect of crystal length on optical conversion. We experimentally studied the conversion efficiencies in BBO crystals with three different lengths (0.5 mm, 1.0 mm, and 2.0 mm) at various pumping intensity. It was found that at low pumping intensities (for example, $I_p \sim 10$ GW/cm^2), the conversion efficiency increases monotonically with the crystal length: the 2.0-mm BBO yields the highest efficiency (25%), the 0.5-mm BBO gives the lowest efficiency (21%), and the efficiency from the 1.0-mm BBO falls above the latter (22%). It is similar to what is predicted by the calculated results as shown in Fig. 8. At sufficiently high pumping intensity ($I \approx 120$ GW/cm^2), at which optimum crystal length is expected to be ~0.6 mm, the shortest BBO (0.5 mm) has the highest SH energy (34%), the 1.0 mm BBO has an efficiency of 30%, and the longest BBO (2.0 mm) produces the lowest efficiency (27%), indicating that the outputs from three crystal lengths fall into the oscillatory behavior as mentioned earlier.

The detailed experimental results on the dependence of the conversion efficiency as a function of pumping intensity measured in the above-mentioned BBO are shown in Fig. 10(a). It can be found from Fig. 10(a) that the optical-conversion efficiency increases monotonically with the pumping intensity when the intensity is between 10 and 25 GW/cm^2. For the case in which the pumping intensity is lower than 10 GW/cm^2, although the data are not presented in Fig. 10(a), it was found that the longer crystal generates higher efficiency and that the SHG efficiency is almost a quadratic function of pumping intensity. The efficiency reaches its maximum at 25–40 GW/cm^2, depending on the thickness of the BBO crystal, and then decreases toward higher intensities. The decrease of efficiency at high intensity is due to the conversion of the SH signal back to the fundamental and to other nonlinear optical effects, such as parametric superfluorescence (see the discussion below). Strong parametric superfluorescence can be seen in all three crystals when the pumping intensity is higher than 50 GW/cm^2. The threshold intensity, at which the superfluorescence

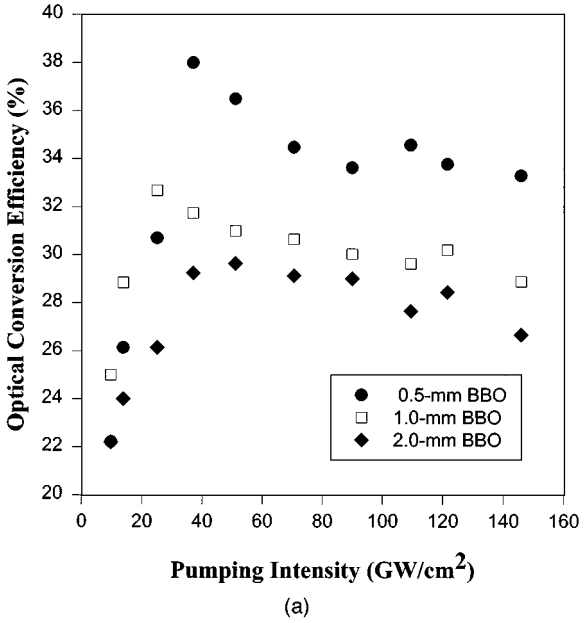

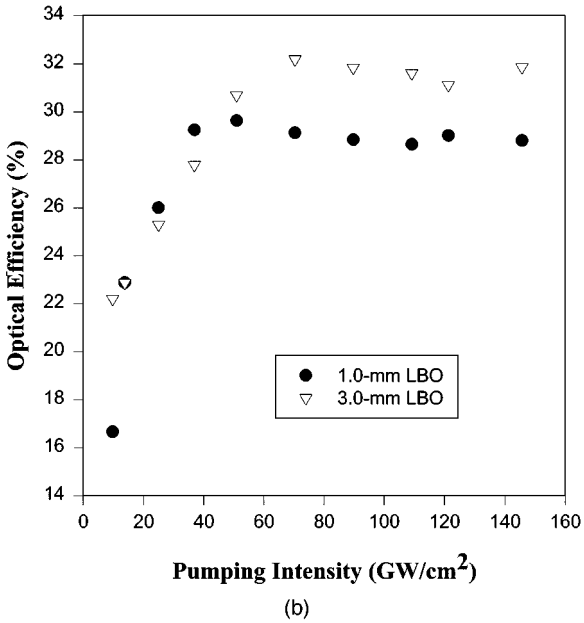

Fig. 10. (a) Experimental measurement of optical-conversion efficiency of SHG in three BBO crystals with different thicknesses as a function of laser pumping intensity. (b) Experimental measurement of optical-conversion efficiency of SHG in LBO as a function of laser pumping intensity.

can be seen, depends on the crystal length. A shorter crystal has a higher threshold intensity. The highest optical efficiency of 38% is achieved in the 0.5-mm BBO at a pumping intensity of ~40 GW/cm^2. Such a high efficiency is achieved without causing significant pulse broadening and degrading of the spectrum. Therefore the optimal crystal length for BBO is ~0.5 mm, which is in accordance with the walk-off limit of the pulses in the crystal as predicted in Figs. 8 and 9. Similar results are also observed in two LBO crystals (1.0 mm and 3.0 mm) as shown in Fig. 10(b). It is seen that the experimental results agree qualitatively with the theoretical calculations: The quantitative discrepancy between the theory and the experiment is probably because the calculation has taken into account the backconversion, but it does not include optical parametric generation, which becomes very strong at high intensities, as will be shown later. It may also be because the estimated parameter of quadratic broadening, $f_2 = 0.2$, used in the calculation may not exactly reveal the real value of f_2. The latter is supported by experimental results of the conversion efficiencies of the three BBO crystals pumped at ~40 GW/cm^2, at which the 1.0-mm BBO is expected to be more efficient than the 0.5-mm BBO, according to the calculated results of Fig. 8, in which $f_2 = 0.2$ is used in the calculation. However, the experimental results show that the efficiency of the 0.5-mm BBO is obviously higher than the other two crystals at such an intensity.

Effect of backconversion, optical parametric processes, and other nonlinear mixings. As mentioned above, when the pumping intensity reaches a certain level, bright and multicolored parametric superfluorescence can be generated in the forward direction within a conical angle. The threshold for generating parametric superfluorescence depends on the crystal length, because the threshold for a crystal decreases as the length of the crystal increases. The conical parametric superfluorescence at high pumping intensity is due to the above-mentioned downconversion and parametric generation, and the spectra are shown in Fig. 11. The spectra was taken by blocking the pump beam and the generated SH beam, which are located at the center of the beam, collecting only the conical emission, and analyzing the spectrum by a CCD spectrometer. One can see clearly from the spectrum that the superfluorescence is mainly formed around two wavelengths: One is due to optical parametric generation in

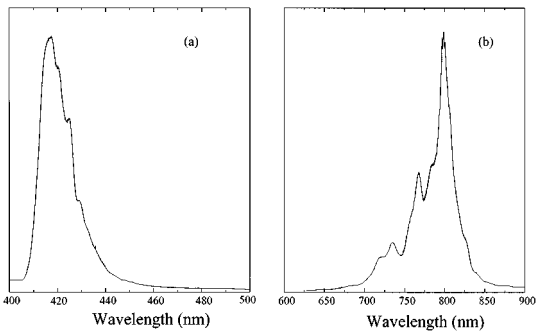

Fig. 11. Experimental spectra of conical parametric superfluorescence in (a) the high-frequency region and in (b) the low-frequency region. The fundamental pumping beam and the generated SHG are spatially filtered out.

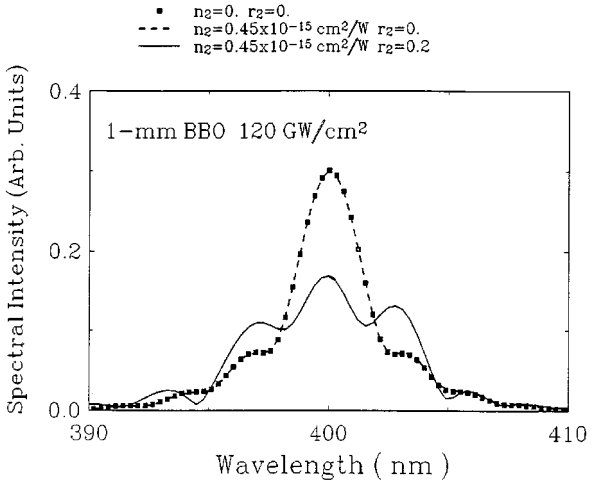

Fig. 12. Calculated SHG spectral profile from a 1-mm BBO at very high pumping intensity with different nonlinear indices of refraction n_2 showing the effect of Kerr nonlinearity. Filled symbols are the result with $n_2 = 0$ and $f_2 = 0$, the dashed curve indicates the result with $n_2 = 0.45 \times 10^{-15}$ cm^2/W and $f_2 = 0$, and the solid curve denotes the result with $n_2 = 0.45 \times 10^{-15}$ cm^2/W and $f_2 = 0.2$.

the crystal with the generated SH pulse at 400 nm because the pump and the radiation are mainly distributed in the red side of the pump (400 nm), covering from 405 nm to more than 460 nm and with a peak wavelength of ~420 nm. The other, near 800 nm, is due to the downconversion of the SH beam from 400 nm back to 800 nm and broadband radiation covering from the visible to the near IR, due presumably to the nonlinear mixing with other components from optical parametric generation. In addition, the beam quality and the spectrum of the generated SH pulses degrade when the above-mentioned higher order nonlinear effects occurred.

Effect of Kerr nonlinearity on the conversion. Since a collimated pump beam with an intensity as high as 150 GW/cm^2 can be readily generated from an amplified ultrashort laser pulse, the self-phase modulation resulting from the optical Kerr effect may affect SH conversion. Figure 12 presents the calculated spectral profiles of the SH wave from a 1-mm-long BBO crystal excited by a 150-fs pulse at 800 nm with different nonlinear indices of refraction and frequency chirping f_2 and with an intensity of 120 GW/cm^2. The filled symbols represent the result with $n_2 = 0$ and $f_2 = 0$, the dashed curve indicates the result with $n_2 = 0.45 \times 10^{-15}$ cm^2/W and $f_2 = 0$, and the solid curve denotes the result with $n_2 = 0.45 \times 10^{-15}$ cm^2/W and $f_2 = 0.2$. As can be clearly seen, the path of the filled symbols, where $n_2 = 0$, $f_2 = 0$, and no Kerr nonlinearity is considered, is almost identical to the dashed curve, where $n_2 = 0.45 \times 10^{-15}$ cm^2/W, $f_2 = 0$, and a severe Kerr effect has been taken into account. It is clear from Fig. 11 that Kerr nonlinearity has very little effect on the output of SHG. On the other hand, the frequency chirping in the fundamental wave plays a much more important role in the SH-conversion process with BBO than that from the optical Kerr nonlinearity, as can be seen by comparing the solid curve with the dashed curve, where both curves have same Kerr nonlinearity ($n_2 = 0.45 \times 10^{-15}$ cm^2/W), whereas the former includes

a frequency chirping of $f_2 = 0.2$. This is understandable considering that in BBO the nonlinear phase variation across the envelope of the fundamental electric field is estimated to be only 0.1π and considering the significant frequency chirping at the pumping intensity used.

From the theoretical and experimental results shown above, one can find that a BBO crystal with a thickness of ~0.5 mm and a medium pumping intensity of ~40 GW/cm^2 are the most favorable to generate SH for ~150-fs pulses. Although it is possible to generate a higher conversion efficiency by use of a longer crystal length (5–10 mm) at a lower pumping intensity, the high efficiency, however, is the price of degradation of temporal and spectral characteristics of the SH output. As has been shown earlier, when the nonlinear interaction length at low pumping level is longer than the pulse walk-off distance, the group-velocity dispersion between the SH and the fundamental waves broadens the SH pulse profile. Therefore when a crystal length longer than the pulse walk-off distance is used, the conversion efficiency increases monotonically with crystal length, but the temporal profile of the generated beam would be broadened. In addition, a thiner crystal, such as a 0.5-mm BBO, also produces a purer SHG spectrum than that of a longer crystal length. High pumping intensity is not recommended because it causes spectral complication that is due to downconversion processes such as DFG and OPG and other nonlinear processes, such as frequency chirping and phase modulation.

4. CONCLUSION

In conclusion, the second-harmonic generation of ~150-fs pulses generated by a commercial regenerative Ti:sapphire laser of ~800 nm in BBO and LBO crystals is investigated both theoretically and experimentally. With a pulse duration of ~150 fs, it was found that the chirping of the fundamental beam and self-phase modulation in the crystal play the most important roles in creating the temporal and spectral degradation and complication in the generated SH pulses. To obtain a high optical-conversion efficiency and to preserve the temporal and spectral characteristics in the generated SH pulses, a thin crystal (for example, a BBO crystal with a thickness of 0.5–0.6 mm, limited mainly by the walk-off) and a moderate pumping intensity (~40 GW/cm^2), at which no parametric superfluorescence is generated, are recommended. A long crystal would result in temporal degradation in the SH pulse because of group-velocity walk-off between the pump and the generated SH pulses and self-phase modulation, while high pumping intensity would create a spectral distortion and complication in the generated SH pulses owing to higher-order nonlinear frequency mixings and other nonlinear effects, such as self-phase modulation and frequency chirping.

5. ACKNOWLEDGMENTS

The experimental work herein was carried out in the Joyce M. Kuok Laser and Photonics Laboratory at Hong Kong University of Science and Technology. This work is sponsored by National Science Foundation under grant PHY-9601922 and the Lightwave Technology Research Programme of the Hong Kong Telecom Institute of Information Technology, and partly by the K. C. Wong Education Foundation of Hong Kong.

REFERENCES

1. W. H. Knox, M. C. Downer, R. L. Fork, and C. V. Shank, "Amplified femtosecond optical pulses and continuum generation at a 5-kHz repetition rate," Opt. Lett. **9**, 552 (1984).
2. P. F. Curley, Ch. Spielmann, T. Brabec, F. Krausz, E. Wintner, and J. Schmidt, "Operation of a femtosecond Ti-sapphire solitary laser in vicinity of zero group-delay dispersion," Opt. Lett. **18**, 54 (1993).
3. M. T. Asaki, C. P. Huang, D. Garvey, J. P. Zhou, H. C. Kapteyn, and M. M. Murnane, "Generation of 11-fs pulses from a self-mode-locked Ti-sapphire laser," Opt. Lett. **18**, 977 (1993).
4. A. Stingl, C. Spiemann, F. Krausz, and R. Szipocs, "Generation of 11-fs pulses from a Ti:sapphire laser without the use of prisms," Opt. Lett. **19**, 204 (1994).
5. J. P. Zhou, G. Taft, C. P. Huang, M. M. Murnane, and H. C. Kapteyn, "Pulse evolution in broadband Ti:sapphire laser," Opt. Lett. **19**, 1149 (1994).
6. J. D. Harvey, J. M. Dudley, P. F. Curley, C. Spiemann, and F. Krausz, "Coherent effects in a self-mode-locked Ti:sapphire laser," Opt. Lett. **19**, 972 (1994).
7. T. R. Zhang, H. R. Choo, and M. C. Downer, "Phase and group velocity matching for second harmonic generation of femtosecond pulses," Appl. Opt. **29**, 3927 (1990).
8. J. Shen, H. He, Y. Liu, Y. Zhang, Z. Wang, and B. Wu, "Second harmonic generation by femtosecond optical pulses: theory and experiment," Chin. Phys. **12**, 413 (1992).
9. A. V. Smith and M. S. Bowers, "Phase distortions in sum- and difference-frequency mixing in crystals," J. Opt. Soc. Am. B **12**, 49 (1995).
10. V. Krylov, A. Rebane, A. G. Kalintsev, H. Schwoerer, and U. Wild, "Second-harmonic generation of amplified femtosecond Ti:sapphire laser pulses," Opt. Lett. **20**, 198 (1995).
11. E. Sidick, A. Knoesen, and A. Dienes, "Ultrashort-pulse second-harmonic generation. I. Transform-limited fundamental pulses," J. Opt. Soc. Am. B **12**, 1704 (1995).
12. E. Sidick, A. Knoesen, and A. Dienes, "Ultrashort-pulse second-harmonic generation. II. Non-transform-limited fundamental pulses," J. Opt. Soc. Am. B **12**, 1713 (1995).
13. D. C. Edelstein, E. S. Washman, L. K. Cheng, W. R. Bosenberg, and C. L. Tang, "Femtosecond ultraviolet pulse generation in β–BaB_2O_4," Appl. Phys. Lett. **52**, 2211 (1988).
14. G. Rodriguez, J. P. Roberts, and A. J. Taylor, "Ultraviolet ultrafast pump-probe laser based on a Ti:sapphire laser system," Opt. Lett. **19**, 1146 (1994).
15. J. Y. Zhang, Z. Xu, Y. Kong, C. Yu, and Y. Wu, "10-HZ, 241 μJ widely tunable parametric generation and amplification in BBO, LBO, and CBO pumped by frequency-doubled femtosecond Ti:sapphire laser pulses," Appl. Opt. (to be published).